PNAS RESEARCH ARTICLE | NEUROSCIENCE

Real-time imaging of *Arc/Arg3.1* transcription ex vivo reveals input-specific immediate early gene dynamics

Pablo J. Lituma[a], Robert H. Singer[b], Sulagna Das[b,1], and Pablo E. Castillo[a,c,1]

Edited by Richard Huganir, Johns Hopkins University School of Medicine, Baltimore, MD; received December 27, 2021; accepted August 4, 2022

The ability of neurons to process and store salient environmental features underlies information processing in the brain. Long-term information storage requires synaptic plasticity and regulation of gene expression. While distinct patterns of activity have been linked to synaptic plasticity, their impact on immediate early gene (IEG) expression remains poorly understood. The activity regulated cytoskeleton associated (*Arc*) gene has received wide attention as an IEG critical for long-term synaptic plasticity and memory. Yet, to date, the transcriptional dynamics of *Arc* in response to compartment and input-specific activity is unclear. By developing a knock-in mouse to fluorescently tag *Arc* alleles, we studied real-time transcription dynamics after stimulation of dentate granule cells (GCs) in acute hippocampal slices. To our surprise, we found that *Arc* transcription displayed distinct temporal kinetics depending on the activation of excitatory inputs that convey functionally distinct information, i.e., medial and lateral perforant paths (MPP and LPP, respectively). Moreover, the transcriptional dynamics of *Arc* after synaptic stimulation was similar to direct activation of GCs, although the contribution of ionotropic glutamate receptors, L-type voltage-gated calcium channel, and the endoplasmic reticulum (ER) differed. Specifically, we observed an ER-mediated synapse-to-nucleus signal that supported elevations in nuclear calcium and, thereby, rapid induction of *Arc* transcription following MPP stimulation. By delving into the complex excitation–transcription coupling for *Arc*, our findings highlight how different synaptic inputs may encode information by modulating transcription dynamics of an IEG linked to learning and memory.

immediate early gene | input specificity | transcription | real-time imaging | endoplasmic reticulum

Significance

Environmental experiences trigger neuronal activity that elicits gene expression in the nervous system. Rapid induction of specific genes known as immediate early genes (IEGs) supports activity-dependent changes of neuronal circuits to ultimately influence animal behavior. However, the cellular and molecular mechanisms controlling how distinct forms of neuronal activity modulate IEG expression remain unclear. The activity regulated cytoskeleton associated (*Arc*) gene is a critical IEG linked to memory. By imaging *Arc* transcription in real time after neuronal activity, we identified how different receptors and signaling pathways influence transcriptional induction and dynamics of an IEG. Our findings provide insights into how information received by distinct synaptic inputs could be encoded by modulating IEG dynamics.

Encoding of salient stimuli through changes in immediate early gene (IEG) expression highlights a crucial aspect of information processing in the brain (1–3). The activity regulated cytoskeleton associated (*Arc*) gene has received wide attention as a critical IEG involved in certain forms of memory (4–6). Transcriptional activation of *Arc* occurs after long-term changes in neurotransmission (7–9), and the *Arc* messenger RNAs (mRNAs) localize to recently activated synapses (7). Local synthesis of Arc protein was suggested to modulate synaptic strength by stabilization of F-actin and endocytosis of AMPA receptors (AMPARs) (10, 11). Therefore, Arc impacts different forms of synaptic plasticity: long-term potentiation and long-term depression (5, 11–14), but see ref. 15, as well as homeostatic synaptic scaling (16). In addition to influencing synaptic functions, evidence for Arc protein regulation of synaptic plasticity related genes is emerging (17, 18). Taken together, these studies emphasize that precise tuning of Arc protein levels is required to support synaptic plasticity and long-term memory. Thus, elucidating the mechanisms controlling the temporal dynamics of *Arc* gene expression is crucial to our understanding of information processing in the brain.

The pattern and location of neuronal activity required for temporal control of IEG expression remains an open question (19–21). Most studies evaluating how neuronal activity is transduced into gene transcription are primarily based on genome-scale analyses (22) or mRNA detection in fixed tissue (7, 19, 23). Modified in situ hybridization approaches identified *Arc* transcribing neurons after a behavioral task or synaptic stimulation (7, 23). In recent years, *Arc* transcribing neurons have been tracked using reporters expressing GFP or dVenus driven by IEG promoters (24–26). However, visualizing the complexity of endogenous *Arc* transcriptional dynamics remains challenging in live tissue. Overcoming such limitation is important for studying how neurons distinctly encode environmental features through changes in IEG expression. To address this unknown and advance gene-imaging technology, we developed a conditional Cre recombinase approach that fluorescently labels endogenous *Arc* mRNAs in mice. Our tagging strategy was able to detect allelic *Arc* transcription in tissue with high temporal sensitivity. Since transcription is the first step of IEG regulation, imaging *Arc* transcription kinetics is a good indicator of how activity is transduced into different temporal patterns of Arc expression.

Author affiliations: [a]Dominick P. Purpura Department of Neuroscience, Albert Einstein College of Medicine, New York, NY 10461; [b]Department of Cell Biology, Albert Einstein College of Medicine, New York, NY 10461; and [c]Department of Psychiatry and Behavioral Sciences, Albert Einstein College of Medicine, New York, NY 10461

Author contributions: P.J.L., R.H.S., S.D., and P.E.C. designed research; P.J.L. and S.D. performed research; P.J.L. and S.D. analyzed data; and P.J.L., R.H.S., S.D., and P.E.C. wrote the paper.

The authors declare no competing interest.

This article is a PNAS Direct Submission.

[1]To whom correspondence may be addressed. Email: pablo.castillo@einsteinmed.edu or sulagna.das@einsteinmed.edu.

This article contains supporting information online at http://www.pnas.org/lookup/suppl/doi:10.1073/pnas.2123373119/-/DCSupplemental.

Published September 12, 2022.

Using acute hippocampal slices from our reporter mouse, we measured the magnitude and temporal kinetics of *Arc* transcription after direct activation of dentate granule cells (GCs) and selective activation of the excitatory synaptic inputs: medial perforant path (MPP) and lateral perforant path (LPP). We found that presynaptic patterns of activity led to distinct temporal dynamics of *Arc* transcription. MPP synapses rapidly and robustly activated *Arc* transcription via a synapse-to-nucleus signal supported by the endoplasmic reticulum (ER) that contributes to nuclear calcium (Ca^{2+}) elevation. In contrast, LPP stimulation resulted in delayed *Arc* transcription and lower nuclear Ca^{2+} rise. Furthermore, we developed an optical stimulation method to trigger *Arc* transcription in GCs and identified the relative contributions of receptors and subcellular signaling in optical- versus synaptic-driven neuronal activity. Our findings strongly suggest that excitation–transcription coupling of IEGs in neurons display input specificity and that compartmentalized neuronal activity may encode specific environmental features in the genome.

Results

Visualizing Real-Time Transcription of Endogenous *Arc* in Live Tissue after Neuronal Stimulation. To monitor gene transcription in real time, we utilized the stem loop technology, whereby mRNAs tagged with multimerized RNA stem loops are detected after synthesis by high-affinity binding of fluorescently labeled coat proteins (27). The endogenous *Arc* gene was tagged by introducing 24 repeats of PBS loops into the 3′ untranslated region (28) that are bound by the coat protein PCP fused to GFP. A mouse line where PCP-GFP expression was designed to be Cre-dependent using loxP sites enabled cell-specific PCP-GFP labeling (Fig. 1*A*). This *PCP-GFP* mouse was then crossed with the PBS-tagged Arc mouse ($Arc^{P/P}$), to generate double homozygous mice ($Arc^{P/P}$ x *PCP-GFP*) for imaging *Arc* mRNA synthesis in live tissue (Fig. 1*A*). Viral delivery of Cre to hippocampal GCs elicited recombination for fluorescent labeling of *Arc* mRNAs. To induce *Arc* gene expression, stimulation of MPP and LPP synapses was confirmed by paired-pulse properties of field excitatory postsynaptic potentials (Fig. 1*B*). Meanwhile, optogenetic activation of the fast kinetics channelrhodopsin variant ChIEF (29) expressed in GCs elicited action potentials (Fig. 1*B*). Using two-photon microscopy, *Arc* transcription was detected as bright fluorescent foci in GC nuclei after neuronal stimulation (Fig. 1*C* and Movie S1). The emergence of fluorescent foci (intensity >10% from nuclear background) indicated de novo transcription of an *Arc* allele (Fig. 1*C*). Basal transcription can be maintained/enhanced by increasing the amplitude of the preexisting allele or by the appearance of the second allele (Fig. 1*C*). Quantification of these transcriptional signatures was designated as total percentage of *Arc* transcribing cells in the imaging field (Fig. 1*C*). As a result, we could interrogate how GC activity induces *Arc* transcription ex vivo in real time with high spatiotemporal resolution.

Stimulation of Proximal and Distal GC Synapses Activates *Arc* with Different Temporal Kinetics. Long-term changes in neurotransmission and epileptic forms of activity at perforant path inputs elicit *Arc* transcription in GCs (7–9). However, the precise impact of perforant path synapses on the temporal kinetics of *Arc* transcription in GC nuclei is unknown. This is a relevant question because these inputs convey functionally distinct information; while proximal MPP inputs encode contextual information, distal LPP inputs carry the content of an experience (30–33).

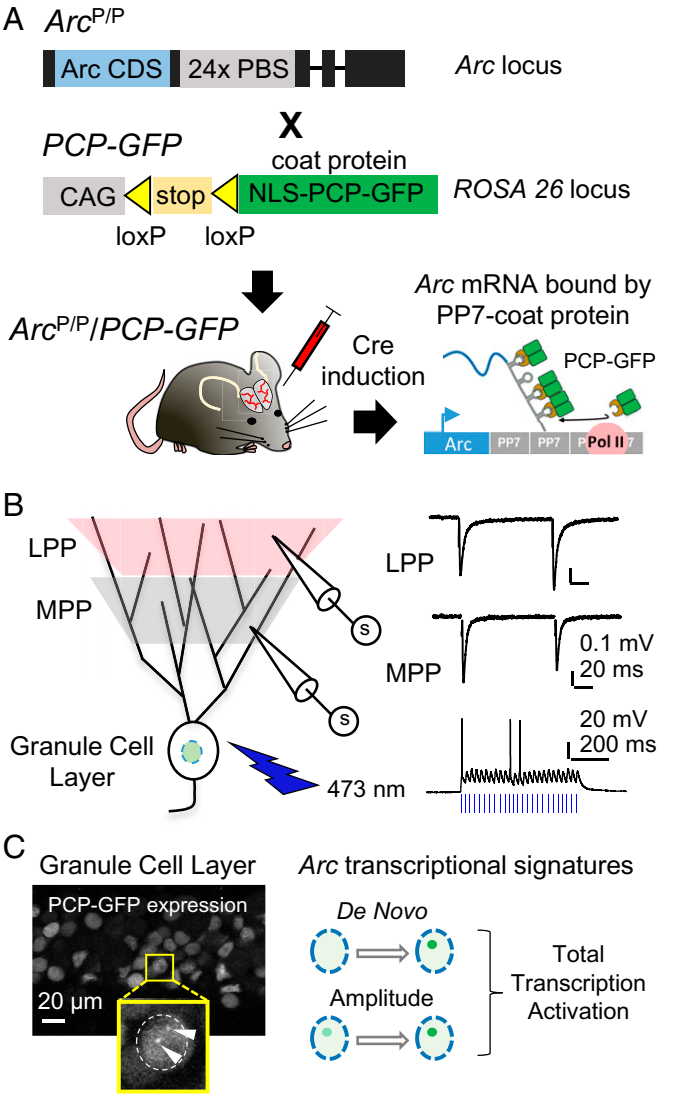

Fig. 1. Cre-inducible *Arc* mRNA tagging system to visualize transcription triggered by neuronal activity in live tissue. (*A*) $Arc^{P/P}$ animals were crossed with *PCP-GFP* transgenic animals that contained PCP-GFP in the *ROSA 26* locus flanked by a stop/lox site rendering PCP-GFP expression Cre-dependent. The double homozygous mouse ($Arc^{P/P}$/*PCP-GFP*) was stereotactically injected with Cre, enabling PCP-GFP binding to the PP7 stem loops on the *Arc* mRNAs and detection of the transcribing alleles. (*B*) (*Left*) Experimental arrangement for the electrical stimulation of LPP and MPP synaptic inputs and optical activation of GCs expressing ChIEF. (*Top Right*) MPP and LPP field excitatory postsynaptic potentials elicited by paired-pulse stimulation and (*Bottom Right*) light-induced action potentials in GCs. (*C*) (*Left*) Representative image shows two transcribing alleles producing tagged *Arc* mRNAs in GCs. (*Right*) Transcription signals were classified as emergence of new (de novo) or increase of basal transcription by enhancement of signal intensity (amplitude) or induction from the second allele. The combined quantification of all signals is denoted as total transcriptional activation.

Hence, we determined how stimulation of MPP or LPP inputs (100 pulses at 200 Hz, repeated five times, interburst interval at 0.2 Hz) regulates *Arc* transcriptional dynamics in real time (Fig. 2*A*). MPP activation significantly induced *Arc* in 12.5 ± 0.6% of the GC population at 15 min and peaked at 30 min (Fig. 2*B*) (*SI Appendix*, Table S1). Conversely, distal LPP stimulation led to *Arc* up-regulation only at later time points (Fig. 2*B*; LPP 8.3 ± 0.9% at 45 min; LPP 9.2 ± 1.1% at 60 min). Unstimulated naïve slices did not exhibit any increase in *Arc* transcription (Fig. 2*B*; naïve 2.6 ± 0.5% at 30 min) (Table S1). To confirm that fluorescent foci reported mRNA synthesis, we imaged slices in the presence of the transcriptional inhibitor DRB (100 μM). Under this

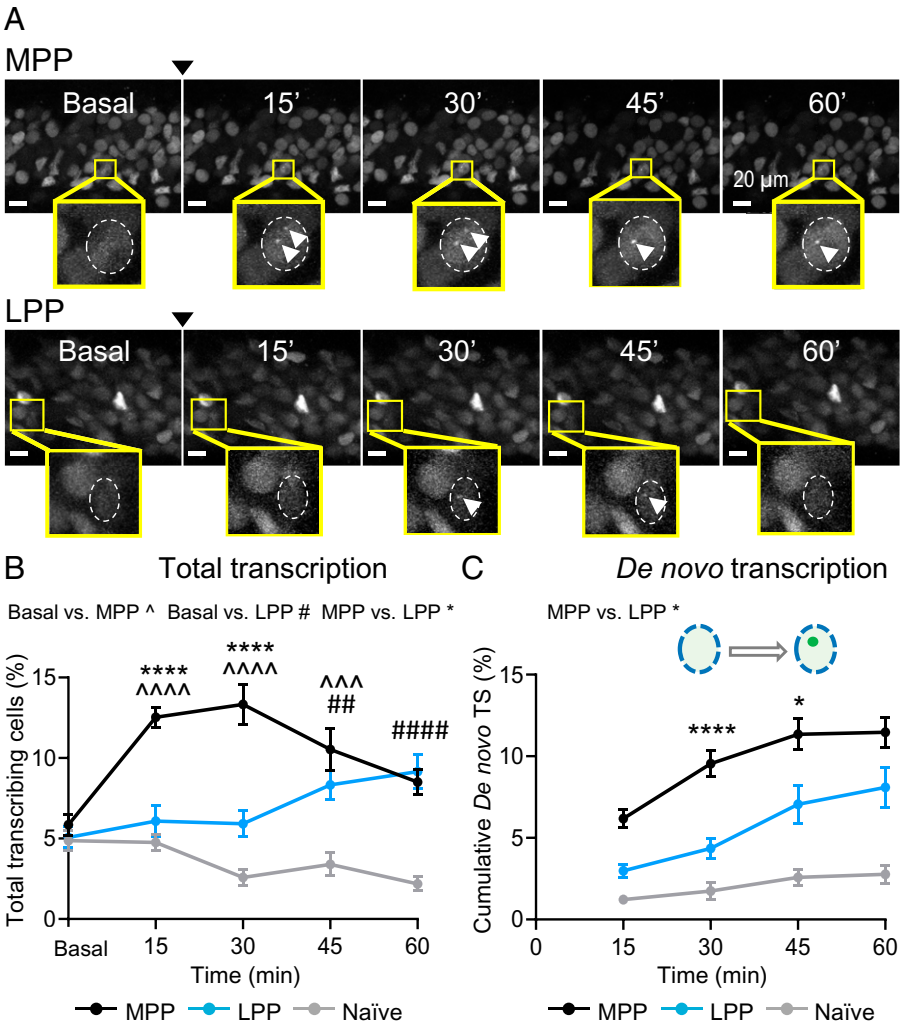

Fig. 2. Electrical stimulation of MPP inputs activates *Arc* transcription with rapid onset as compared to LPP activation. (*A*) Representative time course images of (*Top*) MPP and (*Bottom*) LPP before and after electrical stimulation (denoted by arrowhead). Yellow boxes highlight a GC exhibiting *Arc* transcription in the field of view. (*B*) Quantification of total transcribing cells revealed a significant increase following MPP stimulation (MPP at different time points vs. basal at 0 min; ^^^^$P < 0.001$ at 15 and 30 min; ^^^$P < 0.005$ at 45 min; one-way ANOVA). LPP stimulation led to a significant increase in total transcribing cells at later time points (LPP at different time points vs. basal at 0 min; $^{\#\#}P < 0.01$ at 45 min, $^{\#\#\#\#}P < 0.001$ at 60 min; one-way ANOVA). Early time points of transcriptional activation are significantly different between MPP and LPP (MPP vs. LPP at 15 and 30 min, ****$P < 0.001$, Bonferroni's multiple comparison test). Naïve slices showed no increase in transcription signals. (*C*) MPP elicited larger cumulative de novo transcription as compared to LPP (MPP vs. LPP, ****$P < 0.001$ at 30 min, *$P < 0.05$ at 45 min, Bonferroni's multiple comparison test). In *B* and *C*, naïve nonstimulated slices served as control. MPP, $n = 9$ slices, 7 animals; LPP, $n = 8$ slices, 6 animals; naïve, $n = 6$ slices, 5 animals. Data are presented as mean ± SEM; ****$P < 0.001$, ^^^^$P < 0.001$, $^{\#\#\#\#}P < 0.001$, ^^^$P < 0.005$, $^{\#\#}P < 0.01$, *$P < 0.05$. (Scale bar, 20 µm.)

condition, fluorescent foci were absent, and a decline in total transcribing cells was observed (*SI Appendix*, Fig. S1 *A* and *B*). We also determined the stability of transcription signals postslice preparation that did not vary significantly over time (*SI Appendix*, Fig. S1*C*). After 4 h, we detected transcription foci in 3.9 ± 0.5% of the GC population in fixed tissue (*SI Appendix*, Fig. S1*C*).

To gain deeper insight into activity-dependent *Arc* induction, we selectively quantified GCs displaying de novo transcription. While MPP stimulation elicited immediate early de novo transcription, a significant delay was observed for LPP (Fig. 2*C*; MPP 9.2 ± 0.8% vs. LPP 4.3 ± 0.6% at 30 min). De novo transcription was seen in LPP at 45 min; however, it remained significantly lower than MPP (Fig. 2*C*). Together, these observations strongly suggested that LPP inputs trigger *Arc* transcription with lower efficacy and longer latency than MPP inputs. The proximity of MPP synapses to GC somata could elicit action potentials and thereby influence *Arc* induction kinetics. We excluded this possibility by performing whole-cell current-clamp recordings that revealed repetitive MPP stimulation did not trigger action potentials (*SI Appendix*, Fig. S2*A*). In contrast, LPP stimulation generated action potentials in four out of six GCs with a range of 0 to 10 action potentials (*SI Appendix*, Fig. S2*B*). Weaker recruitment of LPP inputs or a slower synapse-to-nucleus signal could explain differences in temporal kinetics. To address these possibilities, we first increased the number of stimulation bursts that may enhance synapse-to-nucleus signaling (34). Augmenting LPP stimulation in this manner increased charge transfer by threefold but did not accelerate *Arc* transcription (*SI Appendix*, Fig. S3 *A–E*). In an effort to recruit a larger population of LPP inputs, a second stimulation pipette was placed in the synaptic field that increased synaptic charge transfer by fivefold (*SI Appendix*, Fig. S3*B*). We compared total *Arc* transcription and the magnitude of charge transfer and identified a threshold for immediate early *Arc* activation at 15 min (*SI Appendix*, Fig. S3*C*). By recruiting more inputs, we detected a comparable fraction of *Arc* transcribing cells for LPP stimulation as seen for MPP at 30 min (*SI Appendix*, Fig. S3*D*; LPP 2 pipettes 11.2 ± 1.5% vs. MPP 13.3 ± 1.2%) accompanied by an earlier onset of de

novo *Arc* transcription (*SI Appendix*, Fig. S3*E*; LPP 2 pipettes 10.8 ± 1.3% vs. MPP 9.2 ± 0.8%). Strikingly, de novo transcription elicited by two stimulation pipettes in LPP showed a dramatic increase at 45 to 60 min (*SI Appendix*, Fig. S3*E*). Whole-cell patch-clamp experiments revealed that LPP two-pipette stimulation generated a large number of action potentials in all GCs with a range of 24 to 84 action potentials (*SI Appendix*, Fig. S3*F*). Hence, the alteration of transcription kinetics mediated by LPP two-pipette stimulation was, at least in part, due to action potential signaling. Altogether, our observations suggest that the temporal dynamics of *Arc* transcription display input specificity and that enhancing the recruitment of LPP synapses triggers action potentials that accelerate *Arc* induction.

Somatic Action Potential Activity of GCs Elicits *Arc* Transcription. The role of action potential activity in excitation–transcription coupling remains poorly understood (21). Recent evidence indicated that specific forms of neuronal depolarizations impact transcription and translation of selective target genes and proteins, many of which are immediate early in nature (19, 22). Using optogenetic stimulation of GCs, we elicited action potentials and visualized the temporal kinetics of *Arc* transcription (Fig. 3*A*). Quantification of transcription signals after optogenetic stimulation showed that *Arc* was induced within 15 min, with peak values 12.4 ± 1.6% at 30 min, and lasted up to 60 min (Fig. 3*B*). To ensure that ChIEF expression did not result in aberrant up-regulation of *Arc* transcription, we delivered antidromic electrical stimulation to GCs and observed comparable immediate early kinetics (Fig. 3 *B* and *C*). Additionally, we detected changes in amplitude of transcription signals with optogenetic and synaptic stimulation by quantifying allele intensity (*SI Appendix*, Fig. S4). Based on intensity traces of de novo sites, we calculated that activity-induced transcription was maintained for an average of 30 min (*SI Appendix*, Fig. S4), corroborating the ON-duration measured in cultured hippocampal neurons (28). Such observation suggests that the kinetics of the transcriptionally active state may be conserved and intrinsically regulated. Our results established optogenetic stimulation as an effective method to investigate *Arc* transcription in tissue. Accordingly, we sought to determine the stimulation frequencies that induce *Arc* activation by imaging fixed tissue (*SI Appendix*, Fig. S5). By varying the frequency of electrical and optical stimulation we determined that 50-Hz MPP and 25-Hz GC firing is sufficient to trigger *Arc* transcription, respectively (*SI Appendix*, Fig. S5). Taken together, our results indicate that the threshold frequency for *Arc* induction is lower for action potential activity than synaptic stimulation.

Role of Ionotropic Glutamate Receptors and L-Type VGCC in *Arc* Transcription. Neuronal activity can trigger Ca^{2+} influx via different postsynaptic ionotropic glutamate receptors (iGluRs), such as AMPARs and NMDA receptors (NMDARs), or voltage-gated Ca^{2+} channels (VGCCs). Therefore, we determined the impact of these Ca^{2+} sources on the timing and efficacy of *Arc* transcription. MPP stimulation in the presence of the AMPAR antagonist, NBQX (10 μM), and NMDAR antagonist, D-APV (25 μM), significantly reduced *Arc* transcription as compared to control (Fig. 4 *A*, *Top*; MPP 13.3 ± 1.3%; D-APV + NBQX 3.8 ± 1.1% at 30 min). Meanwhile, antagonism of NMDARs alone also prevented a rapid induction of *Arc* transcription for

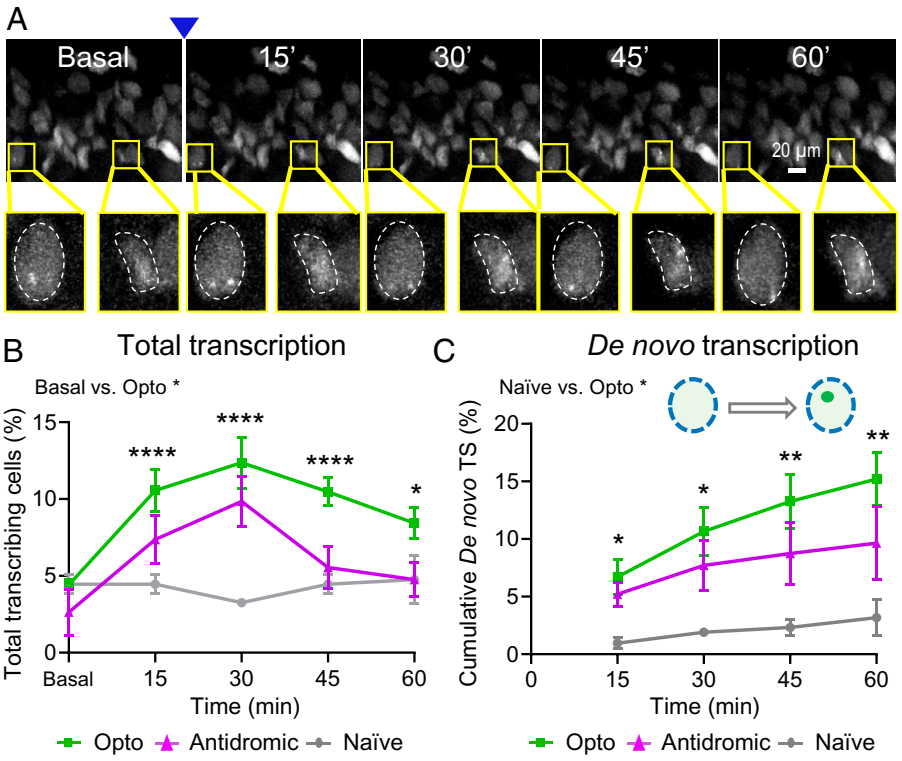

Fig. 3. Optogenetic stimulation of GCs induces *Arc* transcription. (*A*) Representative time course images before and after optogenetic stimulation with 473 nm light (denoted by arrowhead). Yellow box highlights a GC exhibiting *Arc* transcription in the field of view. (*B*) Quantification of total transcribing cells after optogenetic stimulation showed significant *Arc* activation as compared to baseline (Opto vs. basal at 0 min, ****$P < 0.001$ at 15, 30, and 45 min; *$P < 0.05$ at 60 min, one-way ANOVA). Antidromic electrical stimulation of GCs elicits similar *Arc* transcriptional onset as optogenetic activation (Opto vs. antidromic, Bonferroni's multiple comparison test). (*C*) Quantification of de novo transcription following optogenetic stimulation revealed a significant increase as compared to naïve slices (Opto vs. naïve at all time points, $P < 0.05$, Bonferroni's multiple comparison test). Optogenetic and antidromic stimulations display comparable de novo transcription. Opto, $n = 8$ slices, 6 animals. Naïve, $n = 3$ slices, 3 animals. Antidromic, $n = 3$ slices, 3 animals. Data are presented as mean ± SEM; *$P < 0.05$, **$P < 0.01$, ****$P < 0.001$.

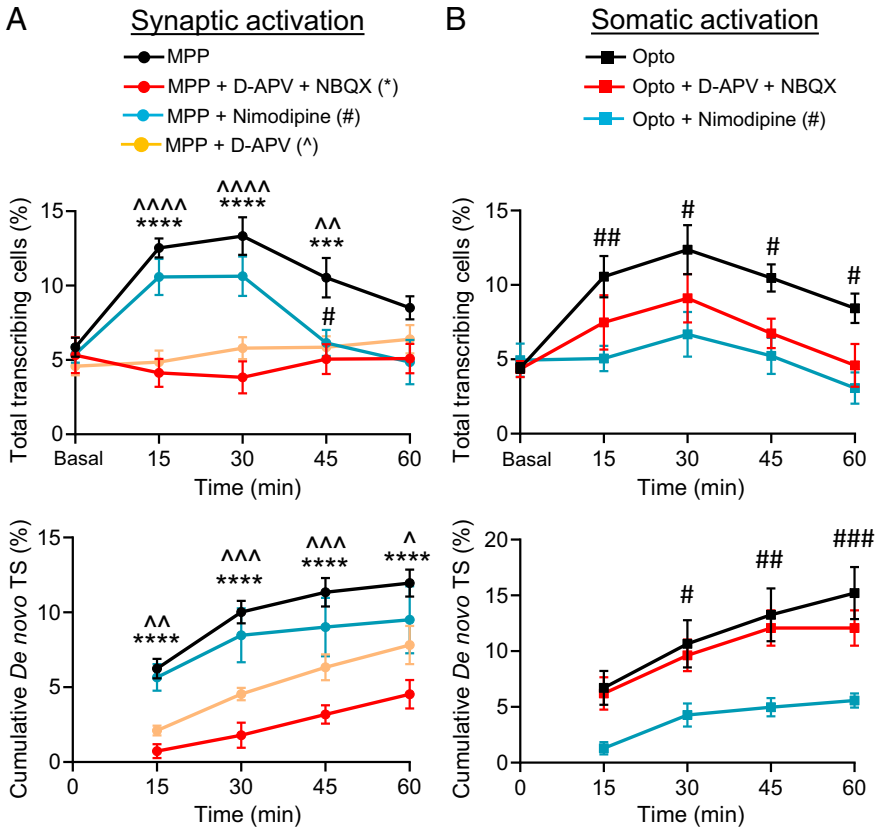

Fig. 4. Contribution of iGluRs and L-type VGCC to *Arc* transcription following synaptic or somatic activation. (*A*) Pharmacological inhibition of iGluRs significantly reduces transcriptional activation as compared to control MPP stimulation (MPP vs. D-APV + NBQX, ****$P < 0.001$ at 15 and 30 min, ***$P < 0.005$ at 45 min, Bonferroni's multiple comparison test). A similar effect was observed with blockade of NMDARs alone (MPP vs. D-APV, ^^^^$P < 0.001$ at 15 and 30 min, ^^$P < 0.01$ at 45 min, Bonferroni's multiple comparison test). L-type VGCC blockade does not impact early *Arc* induction but impaired maintenance at 45 min (MPP vs. Nimodipine, $^{\#}P < 0.05$ at 45 min, Bonferroni's multiple comparison test). De novo transcription exhibits high sensitivity to iGluR antagonism (MPP vs. D-APV + NBQX, $P < 0.005$, Bonferroni's multiple comparison test). MPP, $n = 9$ slices, 7 animals; D-APV + NBQX, $n = 5$ slices, 4 animals; D-APV, $n = 5$ slices, 4 animals; Nimodipine, $n = 6$ slices, 5 animals. (*B*) L-type VGCC blockade attenuates *Arc* transcription after somatic activation (Opto vs. Nimodipine, $^{\#\#}P < 0.01$ at 15 min, $^{\#}P < 0.05$ at other time points, Bonferroni's multiple comparison test). Although iGluR inhibition dampened transcription, it did not have any significant impact on *Arc* induction following somatic activation (Opto vs. D-APV + NBQX, $P > 0.05$, Bonferroni's multiple comparison test). De novo transcription is diminished in the presence of Nimodipine following somatic activation (Opto vs. Nimodipine, $P = 0.05$ at 15 min, $^{\#}P < 0.05$ at 30 min, $^{\#\#}P < 0.01$ at 45 min, $^{\#\#\#}P < 0.005$ at 60 min, Bonferroni's multiple comparison test). Opto, $n = 8$ slices, 6 animals; D-APV + NBQX, $n = 4$ slices, 4 animals; Nimodipine, $n = 5$ slices, 4 animals. Data are presented as mean ± SEM; ****$P < 0.001$, *** $P < 0.005$, $^{\#\#\#}P < 0.005$, ^^^P < 0.005, , $^{\#\#}P < 0.01$, ^^$P < 0.01$, , $^{\#}P < 0.05$, ^$P < 0.05$.

both total and de novo transcription (Fig. 4*A*). The L-type VGCC has been implicated in IEG expression mechanisms (35–37) and is presumably localized to the soma and proximal dendrites of GCs (38). L-type VGCC blockade with Nimodipine (30 μM) had no significant effect on immediate early *Arc* transcription induced by MPP stimulation (Fig. 4 *A*, *Top*; MPP 13.3 ± 1.2%; Nimodipine 10.6 ± 1.2 at 30 min). However, the L-type VGCC may play a role in sustaining transcriptional activation for longer durations (≥45 min) after synaptic stimulation (Fig. 4 *A*, *Top*; MPP 10.5 ± 1.3%, Nimodipine 6.1 ± 0.9% at 45 min). De novo transcription following MPP stimulation was significantly impaired by inhibiting iGluRs (Fig. 4 *A*, *Bottom*) but not with L-type VGCC antagonism (Fig. 4 *A*, *Bottom*). Conversely, optogenetic stimulation activated early *Arc* transcription in the presence of iGluR antagonists, while L-type VGCC blockade caused robust reductions in total and de novo *Arc* transcription (Fig. 4*B*; Opto 12.4 ± 1.6%; Nimodipine 6.7 ± 1.5% at 30 min; Opto de novo 10.7 ± 2.1%; Nimodipine de novo 4.3 ± 1.0% at 30 min). Therefore, the L-type VGCC highly influences *Arc* transcription mediated by somatic activation. To determine how L-type VGCC activity contributes to *Arc* transcription, we assessed the impact of Nimodipine on burst stimulation and cell firing. Our observations did not reveal any major impact on these parameters (*SI Appendix*, Fig. S6) and suggest that Ca^{2+} influx or other signaling cascades may be at play. Although we did not detect a statistically significant effect of iGluR antagonists on optogenetic evoked *Arc* transcription, a trend toward reduction at 45 min was noted (Fig. 4*B*). GC firing can activate hilar mossy cells (MC) that project back onto GCs to constitute the GC–MC–GC autoassociative circuit. Hence, it is not surprising that synaptic activity may partially support action potential–driven *Arc* transcription in autoassociative circuits. Our findings suggest that the Ca^{2+} influx via postsynaptic iGluRs and the L-type VGCC has a distinct contribution to the immediate early activation of *Arc* and transcriptional efficacy depending on the spatial origin of the stimulus.

The ER Facilitates *Arc* Transcription Following MPP Stimulation. The subcellular mechanisms supporting synapse-to-nucleus communication can deeply influence adaptations in gene expression (35, 39–41). To test the involvement of ER-mediated Ca^{2+} wave propagation (42, 43), we depleted intracellular Ca^{2+} stores using the inhibitor of Ca^{2+}-dependent ATPases, cyclopiazonic acid (CPA, 30 μM) (43, 44). CPA strongly attenuated both total and de novo *Arc* transcription after MPP stimulation (Fig. 5*A*; MPP 12.5 ± 0.6%; CPA 6.9 ± 1.1% at 15 min; MPP de novo 6.1 ± 0.5%; CPA de novo 1.5 ± 0.5% at 15 min). Moreover,

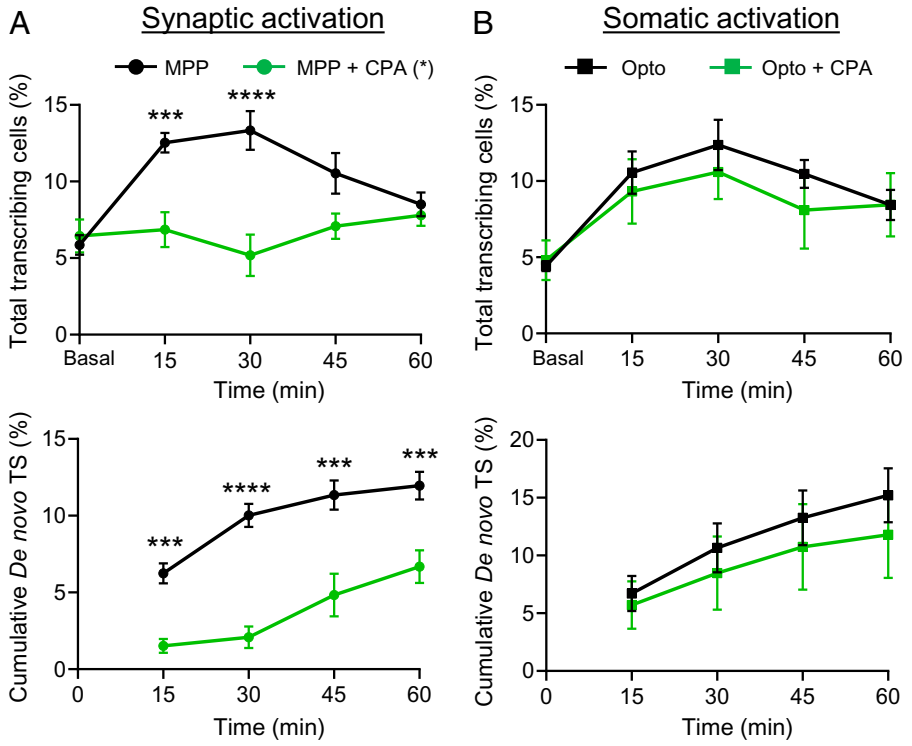

Fig. 5. The ER supports immediate early *Arc* transcription after MPP stimulation. (*A*) Bath application of cyclopiazonic acid (CPA, 30 μM) blocks early phase transcription following MPP stimulation (MPP vs. CPA, ***$P < 0.005$ at 15 and 30 min, Bonferroni's multiple comparison test). CPA treatment attenuates de novo transcription (MPP vs. CPA, ***$P < 0.005$ at 15 min, ****$P < 0.001$ at 30 and 45 min, ***$P < 0.005$ at 60 min, Bonferroni's multiple comparison test). MPP, $n = 9$ slices, 7 animals; CPA, $n = 5$ slices, 5 animals. (*B*) Total and de novo transcription are not impacted by CPA treatment after somatic activation. Opto, $n = 8$ slices, 6 animals; CPA, $n = 4$ slices, 4 animals. Data are presented as mean ± SEM; ****$P < 0.001$, ***$P < 0.005$.

CPA delayed the onset of transcription that remained significantly lower than control (Fig. 5 *A*, *Bottom*). In contrast, CPA had no significant effect on total and de novo *Arc* transcription induced by optogenetic activation (Fig. 5*B*; Opto 10.6 ± 1.4%; CPA 9.3 ± 2.1%; Opto de novo 6.7± 1.5%; CPA de novo 5.7 ± 2.0% at 15 min). To determine the potential contribution of the ER to *Arc* transcription we tested the effect of CPA on burst stimulation and cell firing. Despite observing an increase in charge transfer in CPA conditions (*SI Appendix*, Fig. S6*B*), this effect did not promote *Arc* activation. In contrast, CPA had no impact on cell firing (*SI Appendix*, Fig. S6*E*) indicating ER-mediated Ca^{2+} wave propagation may largely underlie synapse-driven *Arc* induction. Together, these findings strongly suggest that the ER supports a synapse-to-nucleus signal to promote rapid *Arc* transcription during repetitive MPP activity. In contrast, direct activation of GCs that elicits action potentials induces *Arc* transcription that is independent of the ER.

MPP Inputs Elicit Nuclear Ca^{2+} Elevations Supported by the ER. Our observations raised the possibility of ER-mediated Ca^{2+} wave propagation as a synapse-to-nucleus signal supporting *Arc* induction (45–47). To detect nuclear Ca^{2+} elevations in GCs, we expressed a genetically encoded Ca^{2+} indicator containing a nuclear localization signal, NLS-GCaMP6s (Fig. 6 *A* and *B*). Two weeks postsurgery, acute slices were prepared and stimulation of MPP inputs elicited nuclear Ca^{2+} rise (Fig. 6*C*). Subsequent bath application of CPA (30 μM) diminished nuclear Ca^{2+} levels following MPP activity (Fig. 6*C*; MPP 5.6 ± 1.1, CPA 2.9 ± 0.6; total nuclear Ca^{2+}). To discard the possibility that Ca^{2+} reductions were due to photobleaching or repetitive MPP stimulation, we performed successive MPP activations and observed higher Ca^{2+} rise after the second stimulation (Fig. 6*D*; MPP-first 4.3 ± 0.9; MPP-second 6.6 ± 1.6; total nuclear Ca^{2+}). Hence, nuclear Ca^{2+} elevation is supported by the ER and possibly underlies rapid transcription initiation following MPP activation. Given LPP stimulation led to slower transcription kinetics, we sought to determine whether this observation can be explained by the nuclear Ca^{2+} levels induced by LPP synapses. Recruitment of LPP inputs resulted in low nuclear Ca^{2+} levels, while a subsequent MPP activation significantly increased total Ca^{2+} in the same nuclei (Fig. 6*E*; LPP 2.1 ± 0.5; MPP 4.7 ± 1.3; total nuclear Ca^{2+}). Our findings indicate that GC excitatory synapses distinctly elevate nuclear Ca^{2+} levels with MPP inputs specifically eliciting large Ca^{2+} elevations supported by the ER.

Discussion

In this study, we performed high-resolution imaging of *Arc* transcription in real time to elucidate how activity at different spatial locations induces distinct excitation–transcription coupling to regulate *Arc* gene expression in live tissue. We have established that repetitive stimulation of MPP and LPP inputs activate *Arc* transcription in different ways and with unique kinetics (Fig. 7). MPP stimulation strongly induces *Arc* transcription within 15 min, accompanied by increases in nuclear Ca^{2+} that is dependent on ER-Ca^{2+}–mediated signaling. In contrast, LPP stimulation induces a gradual onset of *Arc* transcription that peaks at 45 to 60 min with slower kinetics and lower levels of nuclear Ca^{2+} rise. Input-specific transcription kinetics potentially reflects distinct synapse-to-nucleus signaling mechanisms underlying *Arc* activation. Furthermore, we have characterized the contribution of iGluRs and the L-type VGCC to *Arc* transcription following synaptic (MPP) and somatic activation of GCs. Our results highlight the complex relationship of neuronal activity, nuclear Ca^{2+}, and gene regulation. Importantly, the temporal differences

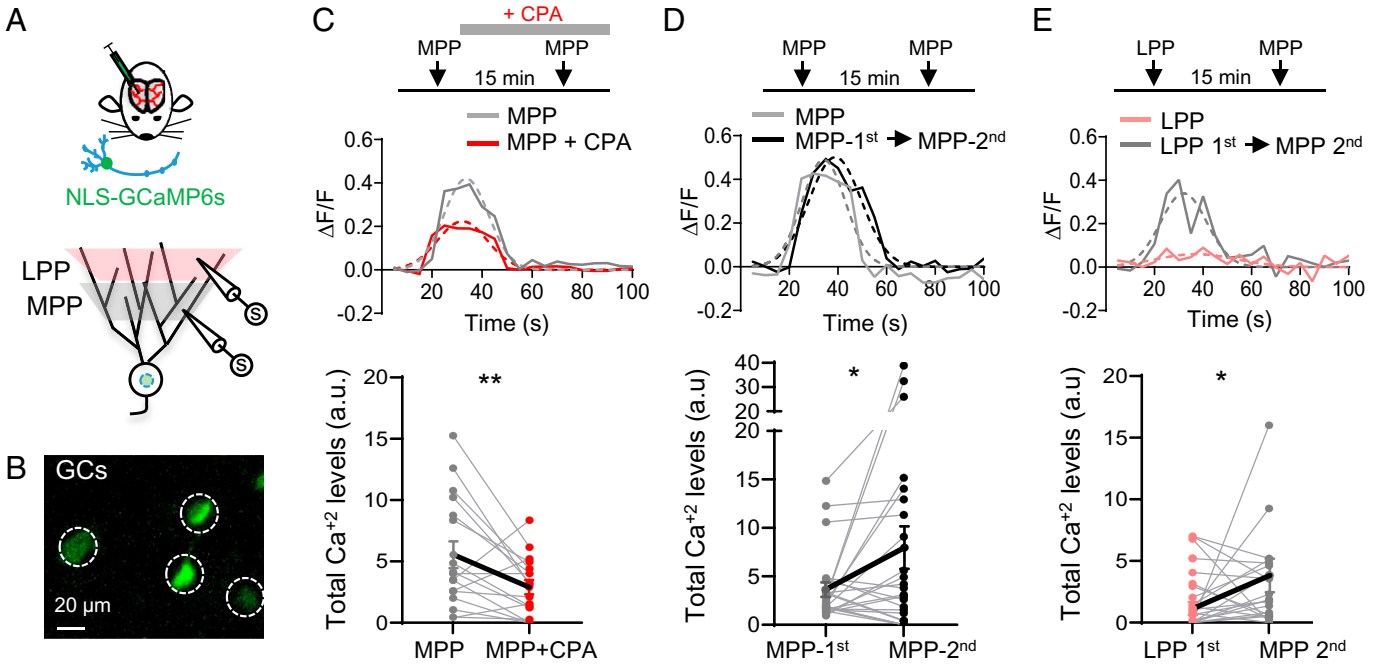

Fig. 6. The ER supports nuclear Ca^{2+} elevations largely driven by MPP synaptic stimulation. (*A*) The genetically encoded Ca^{2+} indicator containing a nuclear localization signal (NLS-GCaMP6s) was injected into the dentate gyrus of $Arc^{P/P}$/*PCP-GFP* mice. Two-weeks postsurgery acute hippocampal slices were prepared for the electrical stimulation of perforant path inputs. (*B*) Image depicting the expression of the NLS-GCaMP6s in GC somata. In panels C-E, the experimental design schematic is represented at the top, line profiles of calcium signals are displayed in the middle, and quantification of total nuclear Ca^{2+} at the bottom (each circle indicates individual nuclei, bold line shows the average). (*C*) CPA treatment (30 µM) significantly reduced nuclear Ca^{2+} rise from baseline MPP stimulation (MPP vs. CPA, $^{**}P < 0.01$, paired *t* test, 17 ROIs; $n = 6$ slices, 4 animals). (*D*) Interleaved experiments revealed nuclear Ca^{2+} increases when MPP inputs are activated repetitively (MPP-first vs. MPP-second, $^{*}P < 0.05$, paired *t* test, 18 ROIs; $n = 7$ slices, 5 animals). (*E*) Stimulation of MPP inputs after LPP activation results in significantly larger nuclear Ca^{2+} signals (LPP vs. MPP, $^{*}P < 0.05$, paired *t* test, 24 ROIs; $n = 6$ slices, 4 animals,). Bold lines indicate mean ± SEM, $^{*}P < 0.05$, $^{**}P < 0.01$.

in subcellular processes that gate IEG transcription in response to GC activity may critically impact hippocampal circuit functions such as learning and memory.

Long-term potentiation, epileptic forms of activity, and memory-related behaviors have been shown to elicit *Arc* transcription in the dentate gyrus of the rodent hippocampus (7–9, 48, 49). Specifically, in situ detection of mRNAs has linked *Arc* transcription to animal behaviors including spatial exploration and gustatory memory (23, 50). However, the ability to persistently track transcription of IEGs in the same neuron in tissue has remained a technical challenge in the field. The development of transgenic mice expressing GFP and dVenus under the *Arc* promoter (24–26) enabled in vivo monitoring of promoter activity (51) but provided an indirect readout of transcription. By tagging the endogenous *Arc* gene, we demonstrate activity-induced transcription with single-allele resolution and detect modes of transcription (amplitude, duration, and de novo activation) in live tissue. Employing electrical and optogenetic stimulation of GCs, we delineate how neuronal activity along the somatodendritic axis influences immediate early *Arc* transcription dynamics. The optogenetic approach may be applied in future work to attain insights into action potential–driven IEG regulation in vivo. The impact of modifying the temporal kinetics of transcription on synaptic plasticity and brain circuit functions remains enigmatic. Future longitudinal studies using this $Arc^{P/P}$*-PCP-GFP* mouse may provide a deeper understanding of IEG dysregulation in maladaptive behaviors associated with brain disorders such as drug addiction, epilepsy, and cognitive decline.

Neuronal activity occurring throughout the somatodendritic axis can differentially impact IEG expression in neurons (21, 35, 40). Recent work on the IEG *Npas4* proposed that neuronal depolarizations in the form of action potentials and excitatory postsynaptic potentials triggered distinct genomic regulation by NPAS4-heterodimers in CA1 pyramidal neurons (19). Although IEGs display commonalities, including activation without the requirement of protein synthesis, each IEG exhibits precise temporal windows of expression (22, 52). In case of *Arc* transcription in the dentate gyrus, our findings revealed similar temporal dynamics following synaptic or somatic activation, although the underlying signaling mechanisms differed (Figs. 4 and 5). Strikingly, synaptic stimulation along the dendritic axis displayed input-specific *Arc* expression. MPP activation resulted in robust and rapid *Arc* transcriptional onset as compared to LPP (Fig. 2). Differences in the latency and magnitude of *Arc* transcription indicate that structural and functional properties of synapses may determine how the same presynaptic activity transduces distinct transcriptional output. Although our results do not fully discard other possibilities, such as differences in synapse distance from the soma, the fact that increasing LPP burst stimulation alone did not alter *Arc* induction suggests that synaptic properties likely influence the threshold for IEG activation. In this regard, we determined that enhanced recruitment of LPP inputs supports rapid onset of *Arc* transcription. Two stimulation pipettes increased the charge transfer by fivefold and led to earlier *Arc* induction at 30 min (*SI Appendix*, Fig. S3). Meanwhile, de novo transcription induced by two pipette LPP stimulation showed a dramatic increase at later time points, 45 to 60 min. Whole-cell patch-clamp experiments revealed that this kinetics was in part due to robust action potential generation (*SI Appendix*, Fig. S3). Our ability to tune transcription onset and kinetics by modifying the recruitment of inputs provides the means to understand activity-dependent transcription regulation with unprecedented resolution. Considering that MPP and LPP

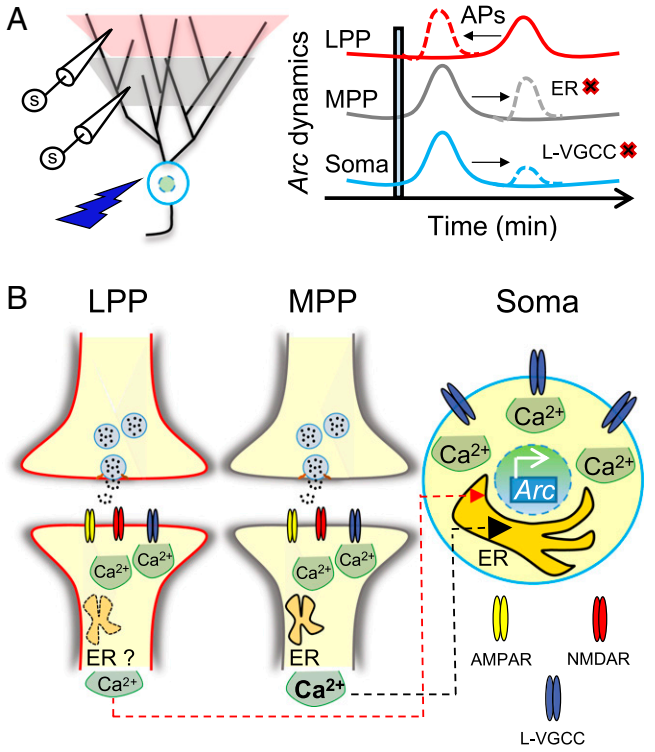

Fig. 7. Synaptic and somatic Ca^{2+} signaling influences *Arc* transcription dynamics in hippocampal dentate GCs. (*A*) Electrical stimulation of synaptic inputs or optogenetic stimulation of the soma (*Left*) elicits distinct *Arc* transcription dynamics (*Right*). Blockade of ER or L-type VGCC (L-VGCC) delays or attenuates *Arc* induction following MPP or somatic stimulation, respectively. LPP stimulation activates *Arc* with delayed kinetics; however, recruiting more inputs and triggering action potentials (APs) can accelerate transcription induction (*Right*). (*B*) Cartoon depicting receptor activation and intracellular signaling in synapses and in soma leading to nuclear Ca^{2+} elevations and *Arc* transcription. LPP stimulation triggers small nuclear Ca^{2+} elevations and slow *Arc* induction, possibly due to reduced ER engagement. In contrast, MPP stimulation leads to robust nuclear Ca^{2+} elevations supported by the ER and rapidly activates *Arc* transcription. Somatic action potentials recruit L-VGCC to engage fast *Arc* dynamics.

mainly convey information about context and content of animal experience, respectively (30–33), our findings may implicate how environmental information processed at different synaptic inputs is uniquely imprinted in the genome to support hippocampal circuit functions.

Synaptic signals are transmitted to the nucleus through several subcellular processes and employ different sources of Ca^{2+} (21, 35, 40, 41, 45). Our results indicate that iGluRs significantly contribute to *Arc* gene activation (Fig. 4) as previously described, albeit using a different stimulation protocol of MPP inputs (7). We identified a potential MPP signaling cascade that engages the ER to elevate Ca^{2+} in the nucleus and induce rapid *Arc* transcription. Depleting ER-Ca^{2+} using CPA strongly attenuated and significantly delayed *Arc* transcription following MPP stimulation (Fig. 5). ER-Ca^{2+} disruption in MPP mirrored the transcriptional kinetics observed by stimulating LPP synapses, suggesting that ER-Ca^{2+} signaling contributes minimally to LPP-driven *Arc* activation, but this possibility requires further testing (Fig. 7). Overall, our findings showcase the contribution of the ER to excitation–transcription coupling following synaptic (MPP) but not somatic activation (Fig. 5). A similar mechanism of Ca^{2+}-induced Ca^{2+} release from the internal stores via ryanodine receptors has recently been reported to up-regulate IEGs like *Npas4* (53). Other signaling cascades, such as MAPK/ERK and BDNF signaling have been implicated in *Arc* activation (54, 55), and these pathways may be operating in concert or independently, depending on the stimulation implemented to induce transcription. In addition, the delayed de novo transcription of *Arc* in the presence of CPA suggests that an alternative slower synapse-to-nucleus mechanism may exist, including activity-dependent shuttling of transcription factors or other proteins from the synapse to the nucleus (41, 56).

MPP stimulation robustly activated *Arc* transcription and generated large nuclear Ca^{2+} elevations, as compared to LPP. Therefore, lower Ca^{2+} rise in the nucleus likely results in slower *Arc* transcriptional activation, as seen following LPP stimulation. Given the synaptic distance of LPP inputs from the GC soma, distal depolarizations may attenuate due to cable properties (57). Recently, NMDAR-mediated plateau potentials and sodium dendritic spikes were shown to robustly impact synaptic plasticity of LPP inputs (58). While dendritic Ca^{2+} spike propagation to the soma can activate the transcription factor *NFAT* (59), whether LPP dendritic spike mechanisms compensate for electrical attenuation to support *Arc* transcription remains to be explored. Nonetheless, our results suggest that MPP and LPP could initiate distinct subcellular processes resulting in different temporal regulation of IEGs to support synaptic plasticity of specific GC inputs. Dissecting the molecular and cellular signaling intricacies of LPP and MPP inputs will further our understanding of how environmental features of content and context are conveyed to the dentate gyrus (30–33).

Our study highlights the importance of revealing the underpinnings of IEG activation that may critically impact brain function. In particular, the possibility of studying IEGs in persistent neuronal populations over time provides opportunities to delve into how compartment- and input-specific activity regulates gene expression in the mammalian brain. While the induction threshold for IEGs like *Arc*, *Npas4*, *c-fos*, and *zif-268* may vary as previously suggested (20), our findings indicate IEG temporal dynamics may be influenced not only by activity but also exhibit input-specificity. The precise neuronal activity required to set in motion cell type–specific gene programs warrants further investigation. Given the implication of IEG dysfunction in brain disorders (46, 60), understanding the temporal kinetics and requirements of IEG expression and their effect on neuronal physiology may provide insights to identify novel therapeutic targets.

Materials and Methods

$Arc^{P/P}$ × PCP-GFP transgenic mouse in a C57BL/6 background (4- to 8-wk-old, both males and females) were used in this study. All animals were group housed in a standard 12 h light/12 h dark cycle and had free access to food and water. Animal handling, breeding, and use followed a protocol approved by the Animal Care and Use Committee of Albert Einstein College of Medicine, in accordance with the NIH guidelines. Experimental procedures, involving *$Arc^{P/P}$ × PCP-GFP* transgenic mouse generation, genotyping, stereotaxic surgery, hippocampal slice preparation, electrophysiology, optogenetics, two-photon microscopy for *Arc* transcription signal detection and for nuclear Ca^{2+} imaging, *Arc* transcription image processing and analysis, nuclear Ca^{2+} imaging analysis, viruses, reagents, and data analysis and statistics, are detailed in *SI Appendix, Supplementary Materials and Methods*.

For more details, refer to *SI Appendix, Supplementary Materials and Methods*.

Data, Materials, and Software Availability. All study data are included in the article and/or *SI Appendix*.

ACKNOWLEDGMENTS. We thank all the P.E.C. and R.H.S. laboratory members for invaluable discussions and Bryen Jordan and Yingxi Lin for critical reading of

our manuscript. We thank Caiying Guo and Janelia Gene Targeting and Transgenics Resources for help with the development of the *PCP-GFP* transgenic mice. We also thank Melissa Lopez Jones for assisting with genotyping and Chiso Nwokafor for animal maintenance. This research was supported by NIH grants R01 NS083085 to R.H.S. and R01 MH125772, R01 MH116673, and R01 NS113600 to P.E.C.; R21 MH122961 to S.D.; and F31MH109267 to P.J.L.

1. J. F. Guzowski, B. Setlow, E. K. Wagner, J. L. McGaugh, Experience-dependent gene expression in the rat hippocampus after spatial learning: A comparison of the immediate-early genes Arc, c-fos, and zif268. *J. Neurosci.* **21**, 5089–5098 (2001).
2. K. Minatohara, M. Akiyoshi, H. Okuno, Role of immediate-early genes in synaptic plasticity and neuronal ensembles underlying the memory trace. *Front. Mol. Neurosci.* **8**, 78 (2016).
3. V. Ramírez-Amaya *et al.*, Spatial exploration-induced Arc mRNA and protein expression: Evidence for selective, network-specific reactivation. *J. Neurosci.* **25**, 1761–1768 (2005).
4. J. F. Guzowski *et al.*, Inhibition of activity-dependent arc protein expression in the rat hippocampus impairs the maintenance of long-term potentiation and the consolidation of long-term memory. *J. Neurosci.* **20**, 3993–4001 (2000).
5. N. Plath *et al.*, Arc/Arg3.1 is essential for the consolidation of synaptic plasticity and memories. *Neuron* **52**, 437–444 (2006).
6. J. E. Ploski *et al.*, The activity-regulated cytoskeletal-associated protein (Arc/Arg3.1) is required for memory consolidation of Pavlovian fear conditioning in the lateral amygdala. *J. Neurosci.* **28**, 12383–12395 (2008).
7. O. Steward, C. S. Wallace, G. L. Lyford, P. F. Worley, Synaptic activation causes the mRNA for the IEG Arc to localize selectively near activated postsynaptic sites on dendrites. *Neuron* **21**, 741–751 (1998).
8. W. Link *et al.*, Somatodendritic expression of an immediate early gene is regulated by synaptic activity. *Proc. Natl. Acad. Sci. U.S.A.* **92**, 5734–5738 (1995).
9. G. L. Lyford *et al.*, Arc, a growth factor and activity-regulated gene, encodes a novel cytoskeleton-associated protein that is enriched in neuronal dendrites. *Neuron* **14**, 433–445 (1995).
10. S. Chowdhury *et al.*, Arc/Arg3.1 interacts with the endocytic machinery to regulate AMPA receptor trafficking. *Neuron* **52**, 445–459 (2006).
11. E. Messaoudi *et al.*, Sustained Arc/Arg3.1 synthesis controls long-term potentiation consolidation through regulation of local actin polymerization in the dentate gyrus in vivo. *J. Neurosci.* **27**, 10445–10455 (2007).
12. J. D. Shepherd, M. F. Bear, New views of Arc, a master regulator of synaptic plasticity. *Nat. Neurosci.* **14**, 279–284 (2011).
13. M. W. Waung, B. E. Pfeiffer, E. D. Nosyreva, J. A. Ronesi, K. M. Huber, Rapid translation of Arc/Arg3.1 selectively mediates mGluR-dependent LTD through persistent increases in AMPAR endocytosis rate. *Neuron* **59**, 84–97 (2008).
14. M. E. Klein *et al.*, Sam68 enables metabotropic glutamate receptor-dependent LTD in distal dendritic regions of CA1 hippocampal neurons. *Cell Rep.* **29**, 1789–1799.e1786 (2019).
15. M. Kyrke-Smith *et al.*, The immediate early gene Arc is not required for hippocampal long-term potentiation. *J. Neurosci.* **41**, 4202–4211 (2021).
16. J. D. Shepherd *et al.*, Arc/Arg3.1 mediates homeostatic synaptic scaling of AMPA receptors. *Neuron* **52**, 475–484 (2006).
17. C. L. Wee *et al.*, Nuclear arc interacts with the histone acetyltransferase Tip60 to modify H4K12 acetylation(1,2,3). *eNeuro* **1**, ENEURO.0019-14.2014 (2014).
18. E. Korb, C. L. Wilkinson, R. N. Delgado, K. L. Lovero, S. Finkbeiner, Arc in the nucleus regulates PML-dependent GluA1 transcription and homeostatic plasticity. *Nat. Neurosci.* **16**, 874–883 (2013).
19. G. S. Brigidi *et al.*, Genomic decoding of neuronal depolarization by stimulus-specific NPAS4 heterodimers. *Cell* **179**, 373–391.e27 (2019).
20. P. F. Worley *et al.*, Thresholds for synaptic activation of transcription factors in hippocampus: Correlation with long-term enhancement. *J. Neurosci.* **13**, 4776–4786 (1993).
21. J. P. Adams, S. M. Dudek, Late-phase long-term potentiation: Getting to the nucleus. *Nat. Rev. Neurosci.* **6**, 737–743 (2005).
22. K. M. Tyssowski *et al.*, Different neuronal activity patterns induce different gene expression programs. *Neuron* **98**, 530–546.e11 (2018).
23. J. F. Guzowski, B. L. McNaughton, C. A. Barnes, P. F. Worley, Environment-specific expression of the immediate-early gene Arc in hippocampal neuronal ensembles. *Nat. Neurosci.* **2**, 1120–1124 (1999).
24. M. Eguchi, S. Yamaguchi, In vivo and in vitro visualization of gene expression dynamics over extensive areas of the brain. *Neuroimage* **44**, 1274–1283 (2009).
25. V. Grinevich *et al.*, Fluorescent Arc/Arg3.1 indicator mice: A versatile tool to study brain activity changes in vitro and in vivo. *J. Neurosci. Methods* **184**, 25–36 (2009).
26. K. H. Wang *et al.*, In vivo two-photon imaging reveals a role of arc in enhancing orientation specificity in visual cortex. *Cell* **126**, 389–402 (2006).
27. H. Sato, S. Das, R. H. Singer, M. Vera, Imaging of DNA and RNA in living eukaryotic cells to reveal spatiotemporal dynamics of gene expression. *Annu. Rev. Biochem.* **89**, 159–187 (2020).
28. S. Das, H. C. Moon, R. H. Singer, H. Y. Park, A transgenic mouse for imaging activity-dependent dynamics of endogenous Arc mRNA in live neurons. *Sci. Adv.* **4**, eaar3448 (2018).
29. J. Y. Lin, M. Z. Lin, P. Steinbach, R. Y. Tsien, Characterization of engineered channelrhodopsin variants with improved properties and kinetics. *Biophys. J.* **96**, 1803–1814 (2009).
30. H. Lee, D. GoodSmith, J. J. Knierim, Parallel processing streams in the hippocampus. *Curr. Opin. Neurobiol.* **64**, 127–134 (2020).
31. C. Wang, X. Chen, J. J. Knierim, Egocentric and allocentric representations of space in the rodent brain. *Curr. Opin. Neurobiol.* **60**, 12–20 (2020).
32. T. H. Hoang, V. Aliane, D. Manahan-Vaughan, Novel encoding and updating of positional, or directional, spatial cues are processed by distinct hippocampal subfields: Evidence for parallel information processing and the "what" stream. *Hippocampus* **28**, 315–326 (2018).
33. E. S. Nilssen, T. P. Doan, M. J. Nigro, S. Ohara, M. P. Witter, Neurons and networks in the entorhinal cortex: A reappraisal of the lateral and medial entorhinal subdivisions mediating parallel cortical pathways. *Hippocampus* **29**, 1238–1254 (2019).
34. C. P. Bengtson, H. E. Freitag, J. M. Weislogel, H. Bading, Nuclear calcium sensors reveal that repetition of trains of synaptic stimuli boosts nuclear calcium signaling in CA1 pyramidal neurons. *Biophys. J.* **99**, 4066–4077 (2010).
35. K. Deisseroth, P. G. Mermelstein, H. Xia, R. W. Tsien, Signaling from synapse to nucleus: The logic behind the mechanisms. *Curr. Opin. Neurobiol.* **13**, 354–365 (2003).
36. T. H. Murphy, P. F. Worley, J. M. Baraban, L-type voltage-sensitive calcium channels mediate synaptic activation of immediate early genes. *Neuron* **7**, 625–635 (1991).
37. J. I. Morgan, T. Curran, Role of ion flux in the control of c-fos expression. *Nature* **322**, 552–555 (1986).
38. J. W. Hell *et al.*, Identification and differential subcellular localization of the neuronal class C and class D L-type calcium channel alpha 1 subunits. *J. Cell Biol.* **123**, 949–962 (1993).
39. T. Kawashima *et al.*, Synaptic activity-responsive element in the Arc/Arg3.1 promoter essential for synapse-to-nucleus signaling in activated neurons. *Proc. Natl. Acad. Sci. U.S.A.* **106**, 316–321 (2009).
40. T. H. Ch'ng, K. C. Martin, Synapse-to-nucleus signaling. *Curr. Opin. Neurobiol.* **21**, 345–352 (2011).
41. B. A. Jordan, M. R. Kreutz, Nucleocytoplasmic protein shuttling: The direct route in synapse-to-nucleus signaling. *Trends Neurosci.* **32**, 392–401 (2009).
42. S. Watanabe, M. Hong, N. Lasser-Ross, W. N. Ross, Modulation of calcium wave propagation in the dendrites and to the soma of rat hippocampal pyramidal neurons. *J. Physiol.* **575**, 455–468 (2006).
43. A. Verkhratsky, Physiology and pathophysiology of the calcium store in the endoplasmic reticulum of neurons. *Physiol. Rev.* **85**, 201–279 (2005).
44. H. B. Kwon, P. E. Castillo, Long-term potentiation selectively expressed by NMDA receptors at hippocampal mossy fiber synapses. *Neuron* **57**, 108–120 (2008).
45. H. Bading, Nuclear calcium signalling in the regulation of brain function. *Nat. Rev. Neurosci.* **14**, 593–608 (2013).
46. E. L. Yap, M. E. Greenberg, Activity-regulated transcription: Bridging the gap between neural activity and behavior. *Neuron* **100**, 330–348 (2018).
47. G. E. Hardingham, F. J. Arnold, H. Bading, Nuclear calcium signaling controls CREB-mediated gene expression triggered by synaptic activity. *Nat. Neurosci.* **4**, 261–267 (2001).
48. M. K. Chawla *et al.*, Sparse, environmentally selective expression of Arc RNA in the upper blade of the rodent fascia dentata by brief spatial experience. *Hippocampus* **15**, 579–586 (2005).
49. A. Vazdarjanova *et al.*, Spatial exploration induces ARC, a plasticity-related immediate-early gene, only in calcium/calmodulin-dependent protein kinase II-positive principal excitatory and inhibitory neurons of the rat forebrain. *J. Comp. Neurol.* **498**, 317–329 (2006).
50. S. N. Burke *et al.*, Differential encoding of behavior and spatial context in deep and superficial layers of the neocortex. *Neuron* **45**, 667–674 (2005).
51. V. Jakkamsetti *et al.*, Experience-induced Arc/Arg3.1 primes CA1 pyramidal neurons for metabotropic glutamate receptor-dependent long-term synaptic depression. *Neuron* **80**, 72–79 (2013).
52. A. E. West, M. E. Greenberg, Neuronal activity-regulated gene transcription in synapse development and cognitive function. *Cold Spring Harb. Perspect. Biol.* **3**, a005744 (2011).
53. P. Lobos *et al.*, RyR-mediated Ca^{2+} release elicited by neuronal activity induces nuclear Ca^{2+} signals, CREB phosphorylation, and Npas4/RyR2 expression. *Proc. Natl. Acad. Sci. U.S.A.* **118**, e2102265118 (2021).
54. E. Messaoudi, S. W. Ying, T. Kanhema, S. D. Croll, C. R. Bramham, Brain-derived neurotrophic factor triggers transcription-dependent, late phase long-term potentiation in vivo. *J. Neurosci.* **22**, 7453–7461 (2002).
55. J. K. Chotiner *et al.*, Assessment of the role of MAP kinase in mediating activity-dependent transcriptional activation of the immediate early gene Arc/Arg3.1 in the dentate gyrus in vivo. *Learn. Mem.* **17**, 117–129 (2010).
56. S. Zhai, E. D. Ark, P. Parra-Bueno, R. Yasuda, Long-distance integration of nuclear ERK signaling triggered by activation of a few dendritic spines. *Science* **342**, 1107–1111 (2013).
57. R. Krueppel, S. Remy, H. Beck, Dendritic integration in hippocampal dentate granule cells. *Neuron* **71**, 512–528 (2011).
58. S. Kim, Y. Kim, S. H. Lee, W. K. Ho, Dendritic spikes in hippocampal granule cells are necessary for long-term potentiation at the perforant path synapse. *eLife* **7**, e35269 (2018).
59. A. R. Wild *et al.*, Synapse-to-nucleus communication through NFAT is mediated by L-type Ca^{2+} channel Ca^{2+} spike propagation to the soma. *Cell Rep.* **26**, 3537–3550.e4 (2019).
60. F. T. Gallo, C. Katche, J. F. Morici, J. H. Medina, N. V. Weisstaub, Immediate early genes, memory and psychiatric disorders: Focus on c-Fos, Egr1 and Arc. *Front. Behav. Neurosci.* **12**, 79 (2018).